International Journal of Rock Mechanics and Mining Sciences 110 (2018) 291–305

Contents lists available at ScienceDirect

International Journal of Rock Mechanics and Mining Sciences

journal homepage: www.elsevier.com/locate/ijrmms

Experimental investigation of the influence of pore pressure and porosity on the deformation of granular salt

Brandon C. Lampe[a,*,1], John C. Stormont[a], Timothy D. Lynn[a,2], Stephen J. Bauer[b]

[a] Department of Civil Engineering, University of New Mexico, Albuquerque, NM, USA
[b] Geomechanics Department, Sandia National Laboratories, Albuquerque, NM, USA

ARTICLE INFO

Keywords:
Granular salt
Effective stress
Inelastic deformation
Localized stress
Isostatic compression

ABSTRACT

The influence of pore pressure and porosity on the ductile deformation of granular salt was experimentally investigated under a isostatic compression at elevated temperatures. Confining and pore pressures were independently controlled while granular salt samples exhibited rate-dependent deformation that resulted in large decreases of sample volume and porosity. Over the experimental durations, which ranged from one to seven days, volumetric strain rates generally ranged from 10^{-2} down to 10^{-10} s^{-1}. The sample deformation rates were observed to correspond with both the sample porosity and the pressure difference between the confining and pore pressures. Experimental results show that the volumetric strain rate decreased when either the sample porosity or the pressure difference were decreased. Post-test observations revealed that the reduced porosity was caused by the solid particles deforming in a ductile manner into the pore volume. Insight into the cause of ductile deformation under isostatic compression was gained by considering the local stress distribution within a sample, which was approximated with the use of a representative volume element. Analysis of the local stress distribution showed how the magnitude of localized shear stress depends on both porosity and the pressure difference, which is consistent with the experimental results.

1. Introduction

Subsurface salt deposits are a proposed medium for nuclear waste storage repositories in the US and Europe, and a crucial component of such repositories are the seals designed to prevent the migration of hazardous gases, brines and water out of or into a repository's access shafts that join surface and subsurface facilities. Granular salt is a proposed sealing material for these shafts at horizons where they penetrate through the in-situ salt units and around waste canisters in disposal rooms.[1] Loose granular salt will be backfilled into these areas, and as external loads, from creep closure of the adjacent salt formation, are applied to the granular salt, it will undergo a sufficient decrease in porosity and permeability such that it acts as a barrier.

Previous studies have shown that a considerable amount of gas may be generated within a subsurface repository from the degradation of stored materials,[2–4] which may elevate pore pressure (P_p) within the void space of a sealed repository. In addition to the generation of gas, P_p may be further amplified within the granular salt backfill as porosity (ϕ) decreases during consolidation and the repository temperature increases from ambient to that of the in situ rock formation.[5] These transient conditions could also result in the pressurization of water present within the host formation (or any other fluid present within the granular salt backfill). The impact of pressurized pore fluid on the consolidation of granular salt has not previously been experimentally investigated, and researchers in the field have only postulated that it may impede consolidation and the ability of granular salt to act as a barrier.[1]

Proper understanding of the phenomena causing the deformation and associated consolidation of granular salt is imperative for the safe design of a repository seal; therefore, knowledge of how P_p influences the deformation of granular salt is needed. Many experimental and theoretical studies have been completed in an effort to understand the deformation of granular salt,[6–10] and practitioners in this field have widely assumed the influence of P_p is accurately described with the effective stress principle as proposed independently by Terzaghi[11] and Fillunger[12]. In essence, this principle states that P_p only influences spherical components of stress within a porous material, and it is often presented in the mathematical form proposed by Biot[13]:

* Corresponding author.
E-mail address: brandon.lampe@wsp.com (B.C. Lampe).
[1] Present Address: WSP USA 3824 Jet Drive, Rapid City, SD 57703, USA.
[2] Present Address: WSP USA 16200 Park Row, Houston, TX 77084, USA.

https://doi.org/10.1016/j.ijrmms.2018.07.007
Received 17 January 2018; Received in revised form 19 July 2018; Accepted 28 July 2018
1365-1609/ © 2018 Elsevier Ltd. All rights reserved.

$$\boldsymbol{\Sigma}' = \boldsymbol{\Sigma} - \alpha P_p \boldsymbol{i} \quad (1)$$

where $\boldsymbol{\Sigma}$ is the total stress tensor, $\boldsymbol{\Sigma}'$ is the effective stress tensor, α is termed Biot's parameter, P_p is the fluid pressure within the connected pore space of the material, and $\boldsymbol{i}$ is the second-order identity tensor. Biot[13] defines $\boldsymbol{\Sigma}$ as the average stress acting on a volume element containing both fluid and solid phases, and this element is sufficiently large to be considered homogeneous. This form of the effective stress principle has been experimentally validated by Nur and Byerlee[14] and many others for fluid-saturated isotropic materials undergoing linear-elastic deformation. However, the applicability of the effective stress principle to inelastic (nonrecoverable) deformation has not been theoretically proven or experimentally validated. Experimentalists considering the ductile deformation of materials typically do not evaluate the influence of P_p; as these materials are often understood to deform according to the von Mises or Tresca yield criteria that only consider the deviatoric components of stress (e.g., cast iron, steel, copper and aluminum,[15] pg. 83)). Consequently, the influence of P_p on the rate-dependent inelastic deformation of ductile materials, such as granular salt, is often overlooked.

This work presents an experimental investigation on how P_p and ϕ influence the ductile deformation of granular salt through a series of isostatic compression (commonly referred to as hydrostatic compression) experiments. Sample deformations were recorded during periods of both transient and creep loading, which allowed for yield to be evaluated during periods of variable and constant (creep) loading conditions. Experiments were performed over a range of pressure and temperature conditions that may exist in a subsurface waste repository. During these experiments confining pressures (), where $P_p < P_c$, ranged from 0 to 38.3 MPa, P_p ranged from 0 to 25 MPa, and samples were subjected to temperatures ranging from approximately 90 to 175 °C.

2. Theory and background

The following subsections present an overview of significant theory and experimental work that forms the current understanding of how of P_p and ϕ influence the ductile deformation of intact and granular salt.

2.1. Investigations on intact salt

Numerous experimental studies, starting in the mid 1970's, have been performed on intact salt; however, the influence of P_p on the deformation of intact salt has largely been ignored. This paucity of experimental work by researchers in the field is understood to result from the common assumption that intact salt is impermeable and not influenced by P_p; however, this is questionable and especially not valid for dilated (damaged) rock salt.[16] The few experimental studies that have evaluated the influence of P_p on the deformation of intact salt have either done so only qualitatively[17,18] or in the context of the poroelastic paradigm of Eq. (1), which requires the determination of α.

For porous materials that are macroscopically isotropic and exhibit linear-elastic deformation, α takes the form:

$$\alpha = 1 - \frac{K_B}{K_S} \quad (2)$$

where K_B and K_S are the drained bulk modulus and unjacketed bulk modulus of the porous material, respectively.[19,20,14] This formulation assumes the pore space is occupied by a single fluid phase of either gas or liquid and the solid phase is incompressible. Experimentally, K_B is determined by measuring the ratio of the to volumetric strain while maintaining a constant P_p (often $P_p = 0$). Whereas K_S is determined in a similar manner but with P_p equal to the , which results in a differential pressure $(P_c - P_p)$ being zero. Because experimentally determining K_S is often difficult, a common assumption is that K_S is exactly the bulk modulus of the solid phase of a porous material, which is theoretically true if the solid phase is composed of a single mineral type.[21] For materials where the solid phase can be considered incompressible relative to the bulk material, which results in bulk volume changes being the consequence of changes in pore volume only, α can be assumed equal to unity; this is often applicable to loose granular materials such as a sand.[22]

McTigue[23] experimentally determined Skempton's B parameter, which relates changes in P_p and under undrained conditions,[24] along with many other bulk properties for rock salt recovered from the Salado formation in southern New Mexico that had $\phi = 0.001$. From the experimentally determined values of $B = 0.93$, $K_B = 20.7\ GPa$, and $K_S = 23.5\ GPa$[23]; $\alpha = 0.128$ was inferred for intact rock salt from the following relationship:

$$\alpha = \frac{K_S - K_B}{BK_S}. \quad (3)$$

This relationship, as provided by Wang,[25] is more general and does not rely on the assumption of an incompressible solid phase to determine α. Both Alkan et al.[26] and Kansy[27] performed experiments on intact and dilated salt from Germany, and their results showed that α ranged from 0.05 to 0.5 for specimen with ϕ less than 0.01. Although these works highlighted the influence of P_p and ϕ on the poroelastic deformation of intact rock salt, no experimental investigations or corresponding theory have been completed to determine the influence P_p and ϕ on the inelastic deformation or inelastic rate-dependent deformation of intact rock salt.

2.2. Investigations on granular salt

Similar to intact salt, experimental work on granular salt began in the 1970's, and this work largely focused on the use of granular salt as backfill material in a waste repository. Because the deformation of both intact and granular salt varies with time, many experimental studies have focused on understanding the rate-dependent deformation of these materials. General observations of how material parameters influenced the volumetric strain rate ($\dot{e}_{vol}$) of granular salt were made by many early researchers in this field. The influence of particle size on the $\dot{e}_{vol}$ was first observed by Shor et al.[28] and Holcomb and Hannum[29, pg. 17] concluded this influence was caused by local stress variations around particle contacts that changed with particle geometry, and the magnitude of this influence was altered as samples deformed.

Holcomb and Shields[30] studied the influence of pore liquid on the consolidation of granular WIPP salt by performing a series of creep tests at an ambient temperature of 30 °C, ranging from 0.69 to 6.9 MPa, and added water content ranging from none to 2.5% of the sample mass. During these tests, flow measurements were intermittently made (with argon gas) to determine sample permeability (k). During this testing, samples were consolidated for durations ranging from 20 to 52 days, and final ϕ values from 0.23 down to 0.06 with k as low as $10^{-20} m^2$ were achieved. Holcomb and Shields[30, pg. 19] noted that in order to measure flow through samples with low k, the argon pressure had to be temporarily increased to $P_p = 5.5$ MPa (while the was 6.9 MPa), which resulted in a transient decrease of the $\dot{e}_{vol}$. A detailed description as to why the $\dot{e}_{vol}$ was influenced by the P_p was not given except for attributing this phenomena to “decreasing the effective ”.

The influence of a pore liquid and particle size on the deformation of granular salt was further evaluated by Spiers et al.[31] where experiments concentrated on understanding the impact of saturating a granular salt sample with a liquid phase (salt brine) during deformation. Creep experiments were performed using a uniaxial consolidation device (oedometer) that allowed for samples to undergo axial (one-dimensional) deformation while lateral deformation was mitigated by a rigid confining cell. Samples were composed of analytical grade sodium chloride with uniform particle sizes, and these samples were tested at 22 °C for up to 20 days under an effective uniaxial stress (Σ'_{unx}), where $\Sigma'_{unx} = \Sigma_{unx} - P_p$. During these experiments, the Σ'_{unx} ranged from 0.5 to 8.0 MPa with a constant $P_p = 1$ atmosphere absolute (0.1 MPa abs.)

applied with saturated brine. Observations on these experiments highlighted how the pore liquid at particle contacts influenced the deformation of granular salt by grain boundary diffusional pressure solutioning. Based on these observed phenomena, Spiers and Brzesowsky[6] developed a micro-mechanical model predicting the $\dot{e}_v$ of fluid saturated granular salt consolidated by the process of grain boundary diffusional pressure solutioning. This model related $\dot{e}_{vol}$ to Σ'_m, where

$$\Sigma'_m = \Sigma_m - P_p = \frac{1}{3}tr(\mathbf{\Sigma}) - P_p. \quad (4)$$

Because the relationship between Σ'_m and $\dot{e}_v$ was only evaluated at a single value of P_p (atmospheric pressure) during uniaxial compression,[6, pg. 87], their proposed relationship may not be generally valid over a range of P_p values.

Influence of the macroscopically applied stress state on consolidation has also been evaluated with traditional triaxial compression devices with $P_p = 0$. Shear experiments on granular salt have been completed by independently varying the maximum principal stress (Σ_1) from the intermediate (Σ_2) and minimum (Σ_3) principal stresses, where $\Sigma_2 = \Sigma_3 = P_c$. For clarification, a macroscopically isotropic stress state is considered here to exist during isostatic compression, where $\Sigma_1 = \Sigma_2 = \Sigma_3$. Accordingly, a macroscopic state of shear exists when the principal stress components are not uniform. Although many experimental works on granular salt have characterized the influence of Σ_m on the $\dot{e}_{vol}$, the influence of macroscopically applied shear stress on granular salt is unclear. Experimental programs completed by Zeuch et al.,[32] Zeuch and Holcomb[33] and Brodsky[34] evaluated the deformation of granular salt under compression, which included both isostatic and shear experiments. These studies concluded that a characteristic difference between the deformation incurred during isostatic and shear experiments did not exist. Contrary to these findings, Callahan et al.[7] stated that samples during shear experiments "exhibit differing behavior depending on the magnitude of the applied stress difference", when referring to the lateral strain rate of samples during shear consolidation; however, no explicit reason is given for why this phenomena is only observed during shear experiments.

Researchers in the European Union have completed numerous in situ and laboratory experiments in an effort to further understand the consolidation of granular salt and in situ rock salt. Notably, the BAMBUS Project included a series laboratory experiments and two in situ experiments located in alternate repository environments, a drift and borehole.[35,36] Results from the in situ experiments provided measurements of temperature, stress, deformation, k, and ϕ in regions backfilled with granular salt. In situ experimental measurements, documented in these works, have been used to validate numerical predictions of granular salt deformation made by numerous constitutive models, and results from these validation efforts have shown that appreciable disagreement exists between the individual constitutive models.

An extensive set of laboratory experiments have been performed by researchers affiliated with the German national project REPOPERM, where the consolidation of granular salt has been investigated under drained conditions at temperatures and pressures relevant to a nuclear waste repository; these experiments primarily consisted of oedometer tests and to a lesser extent traditional triaxial tests.[37,38] Despite the numerous experimental investigations, a general constitutive relation has yet to be developed that adequately describes the long-term consolidation of granular salt, which presumably led Kröhn et al.[38, pg. 58] to consider the influence of local stresses on the macroscopic deformation of granular salt.

Experimental results by Salzer et al.[9, pg. 243] described how while flowing compressed gas through samples of granular salt, to determine k, the deformation was significantly altered in one case. Specifically, Salzer et al.[9] describe how during an isostatic creep test, where $P_c = 10$ MPa and $P_p = 7$ MPa, the sample exhibited a rapid change in the type of deformation as the P_p was increased, from compaction (decreasing bulk volume) to dilation (increasing bulk volume), while the sample was continuously under a macroscopic state of compression. The authors concluded this response showed how the effective stress concept applied to granular salt; however, they did not discuss why a sample under a macroscopic state of isotropic compression would experience dilation.

Although the deformation of granular salt has been a topic of interest for decades, the influence of pore gas pressure on the consolidation of granular salt has not been thoroughly investigated, and very little experimental evidence exists that describes the influence of P_p on the ductile deformation on porous materials in general. In recognition of this and the lack of a consensus on the constitutive relationship between stress and strain for granular salt during creep, it was postulated that P_p has an observable influence on the bulk volumetric deformation of granular salt under isostatic compression, and this influence is the direct result of the existence of substantial ϕ. To evaluate this postulate, P_p was applied during isostatic compression experiments on granular salt while changes in sample bulk volume were measured.

3. Material and methods

3.1. Sample description and preparation

Nine isostatic-compression experiments were performed on samples of granular salt. The sample naming convention was of the form *Temperature_Number*, where *Temperature* represents the targeted sample temperature and *Number* denotes the incremental experiment number. Gaps exist in the value of *Number* because numerous experiments were initiated that had to be ended prematurely because of a wide range of experimental device malfunctions. Table 1 provides the list of experimental results considered here.

Experimental samples consisted of "mine-run" salt that had been excavated from the Salado formation at the WIPP repository. Mine-run salt was sieved such that the maximum particle diameter did not exceed 9.5 mm, a summary of each sample's particle size analysis is provided in the supplemental material associated with this article. The presence of free water (i.e., water not isolated within solid particles) in very small amounts has been observed to influence the deformation of granular salt[39]; therefore, to limit the influence of water on the experimental results, samples were oven dried at 110 °C for over 24 h prior to all experiments.

Each sample consisted of approximately 1.5 kg of granular salt that was placed into a lead jacket lined with copper foil. Placement of the granular salt in the jacket consisted of sequentially creating approximately 2 cm lifts that were lightly tamped to allow for uniform filling of the jacket. The lead jacket was in the shape of a right-circular cylinder with a soldered seam that ran axially along the length of the jacket. The undeformed lead jacket had an approximate length of 23 cm (9 in) with an internal diameter of 10 cm (4 in.). At both ends of the lead jacket were steel end caps, with a diameter of 10 cm (4 in.) and height of 5 cm (2 in.), that held the granular salt in place. A similar approach for jacketing was used by Broome et al.[40] where additional details and

Table 1
Initial and final porosity for each experimental sample.

Sample Identification	Initial ϕ (%)	Final ϕ (%)
90_04	22.1	7.7
90_08	10.6	3.1
175_09	22.6	2.6
175_10	15.3	2.0
175_11	13.4	1.7
175_12	14.3	3.8
175_13	14.1	1.4
175_15	15.0	4.2
175_16	19.0	5.0

further description of the jacketing approach is provided.

3.2. Experimental devices

Experiments were performed at Sandia National Laboratory's Geomechanics Creep Laboratory. Samples were consolidated in a pressure vessel equipped with multiple ports that provided a means to suspend samples, flow test fluids, and run the wires used for data acquisition. was supplied by the application of silicone oil to the exterior of the samples, and the flow of silicone oil was controlled by a Teledyne Isco 500D Syringe Pump. P_p was supplied via an external reservoir of pressurized nitrogen gas that was manually regulated. Ring heaters mounted on the exterior of the pressure vessel were used to supply heat to the sample, and the confining fluid temperature was regulated using measurements from a thermocouple immersed in the confining fluid.

Holcomb and Zeuch[41] showed that the rate-dependent and rate-independent deformation of granular salt was influenced by temperature. The influence of temperature (Θ) on a material's deformation may be considered in terms of a material's melting temperature (Θ_M) when evaluated on an absolute temperature scale. Ashby and Frost[42] showed that many materials deform in a brittle manner when $\Theta \approx 0.1\Theta_M$, but at higher temperatures, where $\Theta \approx 0.5\Theta_M$, the same materials deform in a ductile manner. Temperatures ranging from nominally 90 to 175 °C (363–448 K) were utilized during the experiments described here, where $\Theta_M \approx 800$ °C (1073 K).[43] Therefore, because these experiments were performed at $\Theta \approx 0.34\Theta_M$ to $\Theta \approx 0.42\Theta_M$, deformations were expected to be predominately ductile in nature.

Sample displacements during the experiments were measured with two different methods, (1) metering the confining fluid with the syringe pump and (2) a pair of lateral deformation gages mounted on the exterior of the lead jacket. The primary use of lateral deformation gages was prompted by the extreme sensitivity of confining fluid volume to subtle changes of temperature in the laboratory environment along with the variable compressibility of the confining fluid and the experimental apparatus. The lateral deformations gages were constructed from a metal ring with four high-temperature strain gages adhered to it in a configuration similar to that described by Schuler.[44] The lateral deformation gages had a working range of 2.54 cm with an error of less than five percent over the working range, they were able to provide consistent measurements at temperatures up to 250 °C.

Resolution of the data acquisition system was 0.916 mV, and the lateral deformation gages had an output of 10 V over a 2.54 cm range. Therefore, the greatest possible resolution of the deformation gages was 1.6 μm, which resulted in a minimum detectable change in sample volume of approximately 0.04 cm^3 and a minimum detectable volume strain (e_{vol}) of 5.1×10^{-5}, for a sample with the volume of 700 cm^3. Sample volumes ranged from 1000 cm^3 (initially) down to 700 cm^3 (after consolidation); therefore this estimate of a minimum detectable volume change is conservative. Approximations of the $\dot{e}_{vol}$ were made by determining the time derivative of a smooth function fit to the e_{vol} versus time data.

Based on the minimum detectable e_{vol}, Table 2 provides the required minimum time needed to resolve a specific $\dot{e}_{vol}$. Because of time limitations, the minimum $\dot{e}_{vol}$ reported in this work is not less than $|\dot{e}_{vol}| = 2.5 \times 10^{-10}\ s^{-1}$. The measures of strain reported here are based on the assumption that the sample deformation was isotropic and perfectly captured by the lateral deformation gages (no slipping).

Deformations were also measured with the syringe pump, which had an output range of 10 $volts$ for a fluid volume of 507.38 cm^3. Therefore, when coupled with the data acquisition system, the smallest detectable change in volume from the syringe pump was 0.05 cm^3. Because the density of the silicon oil pumped by the syringe pump was influenced both changes in temperature and pressure, metered volumes from the syringe pump were only utilized during periods of nominally constant temperature and pressure.

Assumptions for isotropic and homogeneous sample deformation were validated by comparing values of the transient sample volume determined with the two fundamentally different measurement techniques (sample diameter with the lateral deformation gages and metering fluid with the syringe pump). That is, volumetric deformations were calculated based on a change in sample diameter measured between two sets of points on the exterior of the sample, and from these deformations, changes in the bulk sample volume were calculated (with the assumptions of isotropy and homogeneity). The calculated bulk sample volume changes as determined by the two sets of external deformation gages were then compared to each other and to the metered change in confining fluid volume under constant pressure and temperature conditions. Measurements reported here from the two deformation gages and the syringe pump were within three percent.

Table 2
Durations needed to resolve volumetric strain rates with lateral deformation gages.

$\dot{e}_{vol}$ (s^{-1})	Duration Needed (h)
10^{-7}	0.15
10^{-8}	1.5
10^{-9}	15.
10^{-10}	150.

3.3. Experimental method

Undeformed samples initially had a bulk volume of approximately one liter with porosities ranging from 30% to 40%. Fig. 1 includes an image of an undeformed sample in part (a). After each sample was assembled, it was placed inside the testing apparatus and preconditioned.

Because granular salt placed within the jacketing material was initially loose and unstable, samples were preconditioned such that they had a stable particle arrangement; this process also resulted in bulk sample deformations that were consistently isotropic. Sample preconditioning was completed in a fashion similar to Brodsky.[34, pg. 31] The process of preconditioning consisted loading the sample, under drained conditions ($P_p = 0$), with a at a rate of 4 MPa/min up to the predetermined and then immediately unloading the sample down to atmospheric conditions (note: sample *175_09* was preconditioned to 14 MPa, all other samples were preconditioned to 20 MPa). Pressure was applied to the samples while at ambient temperature and deformations were not measured during preconditioning (no external gages). After the preconditioning had been completed, samples were removed from the pressure vessel and measurements of the sample mass and volume were made to determine bulk density of the granular salt (ρ_0) prior to each consolidation experiment and ensure that no fluid

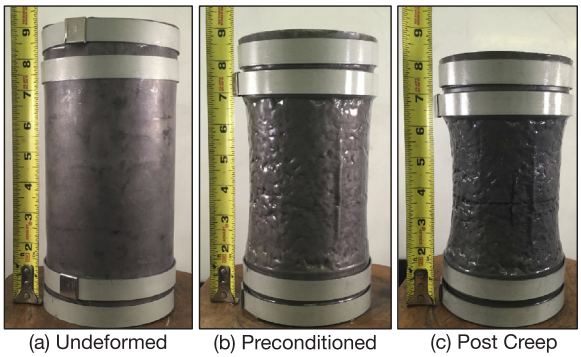

Fig. 1. Pictures of a typical sample at the three stages, (a) undeformed prior to the application of pressure, (b) preconditioned by rapid loading to 20 MPa and unloading under drained conditions, and (c) post consolidation test.

entered the sample during preconditioning. Volume measurements, of the sample when removed from the pressure vessel, were made using two different techniques: (1) calipers were used to measure the external dimensions of the sample and (2) the fluid displaced by the sample when immersed in a calibrated fluid-filled tank. Both of these techniques relied on prior measurements of all non-salt components that made up the sample (lead and copper jackets, end caps, etc.). Results from these two methods were generally in good agreement. Fig. 1 includes an image of the preconditioned sample (prior to the consolidation experiment) in part (b).

Sample density during the consolidation experiments (ρ) was determined based on the ρ_0 and changes in sample volume during each experiment (assuming the mass of granular salt was constant). Sample porosity, during the experiments, was determined by relating ρ to the reference values for density (ρ_{ref}) and connected porosity of in situ rock salt at WIPP, which are 2160 kg/m^3 and zero, respectively.[45,46] Based on these reference values, the ratio of the current interconnected pore volume (V_p) to the current bulk sample volume (V) is termed the bulk sample porosity (ϕ):

$$\phi = \frac{V_p}{V} = 1 - \frac{\rho}{\rho_{ref}}. \tag{5}$$

After each sample had been preconditioned and its initial bulk density had been determined, the sample was placed back into the pressure vessel and heated to the desired experimental temperature. Sample heating was performed with the sample completely submerged in the confining fluid while the upper bleed valve remained open to the atmosphere, which allowed for the confining fluid to be expelled from the pressure vessel as it expanded during the heating process and for the confining fluid to remain unpressurized. Once the confining fluid temperatures had stabilized (nominally 90 or 175 °C) for over 12 h, the upper bleed valve was closed. Fluid pressures were increased at a rates ranging from 1 to 4 MPa/min until the desired pressures (and P_p) were achieved. During these experiments two different loading types employed, *transient* and *creep*. Periods when the pressures continuously changed are referred to as *transient loading*, and periods when the pressures were held constant are referred to as *creep loading*.

3.4. Clarification on terminology

Because the experiments discussed here did not follow common testing procedures, typical terminology for the experimental conditions does not directly apply. Therefore, further clarification on key terms are provided here.

3.4.1. Sample saturation

Because the connected pore space of each sample was filled with a single gaseous phase, and the P_p was regulated by flowing that gaseous phase into to or out of the sample, all experiments performed here were considered to be saturated with dried-gaseous nitrogen or air. Because all samples were oven dried, to remove free water from within the samples, prior to all experiments; the role of water on consolidation is not be discussed here.

3.4.2. Loading conditions

When considering the elastic deformation of porous materials under isostatic compression, the conditions during loading are often described by two limiting cases referred to as *drained* and *undrained*. Drained conditions exist when the P_p remains constant during loading, and undrained conditions exist when the mass of pore fluid remains constant during loading. However, because inelastic deformation was observed to occur during all stages of the completed experiments, terminology developed to describe elastic deformation will not be employed here.

For the experimental results presented here, refers to the macroscopic fluid pressure applied to the outer surface of the sample. P_p refers to the macroscopic gas pressure in the interconnected pore volume of the bulk sample, and P_d is the difference between and P_p. During changes of pressure, and P_p were independently controlled such that or P_p could be modified until the desired value of P_d was achieved.

4. Experimental results

4.1. Overview of reported data

Characterization of the viscoelastic and viscoplastic deformation was achieved by altering the pressures on a sample (i.e., loading and unloading) during an experiment, and for some experiments loading and unloading cycles were completed multiple times. To analyze the deformation characteristics associated with a specific loading condition, *stages* during each experiment were identified. All completed experiments consisted of multiple stages, where each stage represents a period of time when the sample was subjected to either a continuously variable (transient) or constant (creep) pressure. Transient loading occurred when the and/or P_p continuously varied, and creep loading occurred when both and P_p were held constant. The duration of each stage was determined based on both the availability of experimental equipment and by the rate of sample deformation. In general, when the rate at which the sample volume change was indistinguishable, the experiment was ended.

Deformation of experimental samples was quantified in terms of the bulk volume strain (e_{vol}), which is considered positive in compression (decreasing volume). Finite strain, defined in terms of the natural logarithm of the determinant (det) of the deformation gradient ($\boldsymbol{F}$), was chosen to represent the deformation as given in Eq. (6).

$$e_{vol} = -ln(det[\boldsymbol{F}]) = ln\left(\frac{V^0}{V}\right) \tag{6}$$

Here, V and V^0 represent the deformed and undeformed configurations, respectively. The preconditioned bulk sample volume is considered the undeformed configuration. Because the experimental samples exhibited nonlinear deformation characteristics (i.e., $\dot{e}_{vol}$ varied with ϕ), sample deformation is presented here in terms of ϕ and $\dot{e}_{vol}$, rather than in terms of e_{vol}.

4.2. Experimental loading and deformation data

Results for experiments *90_04, 175_09, 175_10, 175_11, 175_15* and *175_16* are presented here, while results for *90_08, 175_12* and *175_13* are provided in the supplemental material associated with this article. Tables 3–8 list the experimental stages along with the associated pressure conditions and stage durations. During periods of transient loading, the initial and final pressure conditions are presented; however, during periods of creep only the initial pressure conditions are presented. Results are illustrated in Figs. 2–7, where pressures (, P_p and P_d), temperature (Θ), porosity (ϕ) and bulk volumetric strain rate ($\dot{e}_{vol}$) are plotted against the experiment duration.

Fig. 2 illustrates the results of experiment 90_04, which exemplify a traditional creep experiment on granular salt, where pressure is applied to the sample and held constant. During this experiment, was initially raised to 20 MPa and held for the experiment duration while P_p was held at zero. These results show ϕ decreasing with time from an initially large value to a substantially smaller final value along with a continuously decreasing $\dot{e}_{vol}$. These observations are similar to other experiments that consisted of a single transient loading stage followed by creep loading stage, such as 175_16 (Fig. 7).

The rate at which granular salt deforms while under a constant stress has been shown to increase with Θ,[39,6] and this same trend was observed during the experiments described here. Results from 90_04 and 175_16, which were executed at nominally 90 °C to 175 °C,

Table 3
Summary of experiment 90_04.

Stage	Loading	Initial Conditions			Final Conditions			Stage Time	
		P_c (MPa)	P_p (MPa)	P_d (MPa)	P_c (MPa)	P_p (MPa)	P_d (MPa)	Start (day)	Duration (day)
1	Transient	0.0	0.0	0.0	20.0	0.0	20.0	0.000	0.004
2	Creep	20.0	0.0	20.0		———		0.004	4.736
					Total Experiment Time (day):				4.740

respectively, provide a convenient comparison. Both experiments were completed with $P_c = 20$ and $P_p = 0$ MPa, while 175_16 sustained a greater $\dot{e}_{vol}$ for a larger period of time than 90_04. This resulted in the ϕ of 175_16 falling below 0.06 within the first 12 h of the experiment while the ϕ of 90_04 remained above 0.06 over the entire 4.74-day experiment duration.

Most experiments performed here consisted of numerous stages where both and P_p were varied multiple times, which resulted in samples being subjected to a wide range of P_d, as illustrated in Fig. 3. By varying the P_p while holding constant, a determination of which pressure influenced the deformation could be made by monitoring the $\dot{e}_v$. Results from experiment 175_09 show how the $\dot{e}_{vol}$ depended on the P_d, where under constant the $\dot{e}_{vol}$ exhibits a transient increase as the P_d increases (P_p decreases). Alternatively, Fig. 6 (experiment 175_15) illustrates a systematic decrease of $\dot{e}_{vol}$ as the P_d was decreased over multiple stages.

During experiment 175_10 (Fig. 4), a simultaneous change of and P_p was attempted, during Stage 3, such that the P_d would remain at 20 MPa; however, the was decreased at a slightly faster rate than the P_p and this caused a momentary decrease of P_d down to 12 MPa. This decrease of , while briefly holding P_p constant, resulted in a sudden reversal of the deformation (increase of sample volume), as illustrated by the negative $\dot{e}_{vol}$.

Another example of volumetric expansion while under a macroscopic state of compression was observed during stages 9 and 10 of experiment 175_11 (Fig. 5). Where, beginning in Stage 7, the P_d was abruptly increased from 10 to 30 MPa by dropping the P_p to zero, and this event resulted in a rapid decrease of ϕ from 0.07 to 0.04. Following this, the P_p was increased from zero up to 25 MPa over Stages 9 and 10, and the corresponding P_d was dropped to 5 MPa. These conditions were then held during Stage 11 for over 36 h, and during this time the sample exhibited consistent volumetric expansion, which is shown by the negative $\dot{e}_{vol}$ during this time. This transient reversal of the deformation following a decrease of P_d indicates that granular salt has viscoelastic characteristics that depend in part on P_d.

4.3. Post-experiment analysis of deformation

Following each consolidation experiment, samples were removed from the pressure vessel and the external dimensions of the samples was recorded. These results, along with measurements made during each experiment, confirmed that the bulk sample deformation was isotropic. Visual examinations were also completed post experiment by cutting samples, with a diamond saw, into subsections. Fig. 8 illustrates a sample that was consolidated at 175 °C with $P_c = 20$ MPa.

After samples had been divided into subsections, thin sections were made and photomicrographs were taken. Images in Fig. 9 are of consolidated granular salt samples that were deformed at 90 °C under $P_c = 20$ MPa. Samples shown in Fig. 9 had an initial ϕ of nominally 0.20, and are shown here in their post-experiment state with ϕ ranging from 0.08 to 0.03. Much of the pore space observed in Fig. 9 part *a* is located along the intergranular region between adjacent particles; however, when viewed under greater magnification, as in parts *b* and *c* of Fig. 9, the presence of isolated volumes of intragranular pore space is made apparent; these observations are consistent with those made by Pennock et al.[47].

The reduction of ϕ during isostatic compression was observed here to result from local heterogeneities, in the form of void space, around the solid particles in the bulk material. These local heterogeneities caused the stress field to be locally altered from the macroscopically applied isotropic stress. This alteration in stress resulted in the development of shear stresses that caused the solid particles to deform in a

Table 4
Summary of experiment 175_09.

Stage	Loading	Initial Conditions			Final Conditions			Stage Time	
		P_c (MPa)	P_p (MPa)	P_d (MPa)	P_c (MPa)	P_p (MPa)	P_d (MPa)	Start (day)	Duration (day)
1	Transient	0.0	0.0	0.0	13.9	0.0	13.9	0.000	0.009
2	Creep	13.9	0.0	13.9		———		0.009	0.966
3	Transient	13.9	0.0	13.9	22.0	8.0	14.0	0.975	0.009
4	Creep	22.0	8.0	22.0		———		0.984	1.036
5	Transient	22.0	8.0	22.0	22.0	4.0	18.0	2.020	0.007
6	Creep	22.0	4.0	18.0		———		2.027	0.923
7	Transient	22.0	4.0	18.0	22.0	0.0	22.0	2.950	0.015
8	Creep	22.0	0.0	22.0		———		2.965	1.010
9	Transient	22.0	0.0	22.0	30.0	8.0	22.0	3.975	0.010
10	Creep	30.0	8.0	22.0		———		3.985	1.000
11	Transient	30.0	8.0	22.0	30.0	4.0	26.0	4.985	0.014
12	Creep	30.0	4.0	26.0		———		4.999	0.991
13	Transient	30.0	4.0	26.0	30.0	0.0	30.0	5.990	0.010
14	Creep	30.0	0.0	30.0		———		6.000	1.090
					Total Experiment Time (day):				7.090

Table 5
Summary of experiment 175_10.

Stage	Loading	Initial Conditions			Final Conditions			Stage Time	
		P_c (MPa)	P_p (MPa)	P_d (MPa)	P_c (MPa)	P_p (MPa)	P_d (MPa)	Start (day)	Duration (day)
1	Transient	0.0	0.0	0.0	20.0	0.0	20.0	0.000	0.007
2	Transient	20.0	0.0	20.0	30.0	10.0	20.0	0.007	0.026
3	Creep	30.0	10.0	20.0		———		0.033	1.062
4	Transient	30.0	10.0	20.0	20.0	0.0	20.0	1.095	0.040
5	Creep	20.0	0.0	0.0		———		1.135	3.840
					Total Experiment Time (day):				4.975

ductile manner into the pore volume. This phenomenon is depicted by all three images in Fig. 9, where the initially distinct solid salt particles meld into each other as they flow into the adjacent pore space. The observation that pore volume reduction during isostatic compression was the result of ductile deformation was also observed by Mowar et al.[48] on porous limestone, where ductile deformation preceded the onset of cataclasis.

5. Discussion

Key findings from these experiments pertain to the influence of P_p and ϕ on the ductile deformation of granular salt, which had not previously been thoroughly investigated. The isostatic compression experiments presented here were completed with the use of only and P_p, which implies all samples were under a macroscopically uniform state of stress. However, the assumption that an isotropic state of stress exists throughout a porous sample is recognized to be inaccurate and not useful for understanding the cause of ductile particle deformation as observed here; therefore, the concept of a local stress will be utilized to discuss the observed of influence of P_p and ϕ on the inelastic deformation of granular salt.

5.1. Deformation during loading

Deformation during periods of transient loading (prior to creep) has often been neglected when characterizing viscous geologic materials such as salt (e.g., Munson and Dawson,[49] Munson et al.,[50] Callahan[39]). However, results presented here show that an appreciable amount of deformation occurred during these transient loading periods, and if the deformation during transient loading is ignored, this neglect may have significant influence on constitutive parameters. Troyer et al.[51] compared their experimental results to model predicted deformations of a viscoelastic soft porous tissue, where two different sets of model parameters were used, (1) a set of parameters that were fit to data that included periods of loading, and (2) a set of parameters fit to the same data but with periods of loading removed. Troyer et al.[51] concluded that deformation during transient loading cannot be ignored if one is to accurately predict transient material behavior. Recognizing this, deformation during transient loading is considered here.

Experimental results showing the initial-transient loading prior to creep during experiments *175_09, 175_10, 175_11, 175_12, 175_13* and *175_15* are provided in Fig. 10 [3]. Each graph in the figure is on a similar scale to allow for a visual comparison of the , P_p and ϕ during the initial transient loading; additionally, the number inside the *gray* square and vertical lines in each graph identify the particular stage of the experiment. Samples *175_09*, *175_10*, and *175_15* were monotonically loaded during Stage 1 with while P_p was held at 0 MPa, and the measured decrease of ϕ during these experiments was directly related to the increase in . Alternatively, sample *175_13* was subjected to multiple transient load cycles, where was increased and decreased, and the change in ϕ during the unloading in Stages 2 and 4 was negligible. Because the ϕ did not return to the original value upon unloading, this

Table 6
Summary of experiment 175_11.

Stage	Loading	Initial Conditions			Final Conditions			Stage Time	
		P_c (MPa)	P_p (MPa)	P_d (MPa)	P_c (MPa)	P_p (MPa)	P_d (MPa)	Start (day)	Duration (day)
1	Transient	0.0	0.0	0.0	10.0	0.0	10.0	0.000	0.002
2	Creep	10.0	0.0	10.0		———		0.002	0.002
3	Transient	10.0	0.0	10.0	20.0	10.0	10.0	0.004	0.002
4	Creep	20.0	10.0	10.0		———		0.006	0.010
5	Transient	20.0	10.0	10.0	30.0	20.0	10.0	0.016	0.003
6	Creep	30.0	20.0	10.0		———		0.019	0.921
7	Transient	30.0	20.0	10.0	30.0	0.0	30.0	0.940	0.010
8	Creep	30.0	0.0	30.0		———		0.950	0.010
9	Transient	30.0	0.0	30.0	30.0	20.0	10.0	0.960	0.060
10	Transient	30.0	20.0	10.0	30.0	25.0	5.0	1.020	0.020
11	Creep	30.0	25.0	5.0		———		1.040	1.806
13	Transient	30.0	25.0	5.0	30.0	0.0	30.0	2.846	0.019
14	Creep	30.0	0.0	30.0		———		2.865	3.065
					Total Experiment Time (day):				5.930

[3] Results from 175_16 have been omitted here because they were similar to 175_15.

Table 7
Summary of experiment 175_15.

Stage	Loading	Initial Conditions			Final Conditions			Stage Time	
		P_c (MPa)	P_p (MPa)	P_d (MPa)	P_c (MPa)	P_p (MPa)	P_d (MPa)	Start (day)	Duration (day)
1	Transient	0.0	0.0	0.0	20.0	0.0	20.0	0.000	0.005
2	Creep	20.0	0.0	20.0		———		0.005	1.055
3	Transient	20.0	0.0	20.0	20.0	5.0	15.0	1.060	0.020
4	Creep	20.0	5.0	15.0		———		1.080	2.010
5	Transient	20.0	5.0	15.0	20.0	10.0	10.0	3.090	0.009
6	Creep	20.0	10.0	10.0		———		3.099	3.841
					Total Experiment Time (day):				6.940

is evidence the deformation was inelastic. Also notice that upon reloading during Stage 3, negligible deformation occurred until the previous maximum value of (from Stage 1) had been exceeded, this indicates that granular salt strain hardens as its ϕ decreases.

The two graphs in the middle row of Fig. 10 show how samples 175_11 and 175_12 were loaded during Stage 1 with and then during Stage 3 with both and P_p, such that P_d was held approximately constant at 10 MPa. During Stage 3 of these experiments, when and P_p were simultaneously altered, decreases of ϕ were less than 0.05. These changes in ϕ were much less than what was exhibited during Stage 1 of experiments 175_09, 175_10 and 175_11, where samples were loaded to a similar magnitude of but with $P_p = 0$ (ϕ decreased by more than 0.10). This indicates the deformation measured during loading was predominately dependent upon P_d rather than solely or P_p.

To further illustrate the dependence of deformation on P_d, consider the plot shown on the right side of Fig. 11, where a schematic idealization of ϕ and P_d values during a consolidation experiment on granular salt are shown. Here, the concept of a *yield surface* is introduced, which is used here to identify the locus of yield stresses in the $\phi - P_d$ space. The initial magnitude of P_d is identified by ①, which is inside the yield surface. Upon loading, from ① to ②, the deformations is small and reversible (i.e., changes in ϕ are negligible) until the P_d reaches the yield surface at ②. Upon reaching the yield surface, plastic deformation ensues and changes in ϕ become appreciable, and continued decrease in sample ϕ occurs as P_d is increased from ② to ③. At ③, P_d is held constant, but ϕ continued to decrease from ③ to ④ as the sample undergoes continued inelastic deformation under creep conditions. The decrease in ϕ from ③ to ④ results in continued hardening (increase in the stress level associated with plastic strain). Conceivably, if a sample remains under these conditions for a sufficient length of time, such that ϕ approached zero, the yield surface depicted here would approach a horizontal line. This implies a sample with zero ϕ would respond in an elastic manner under a macroscopically isotropic stress regardless of the P_d. Further discussion of these concepts will be provided in Section 5.2.

With these ideas in mind, consider the remaining two plots on the left in Fig. 11 that illustrate the data from Fig. 10 in terms of ϕ and pressure. On these graphs, ϕ is plotted against two different measures of

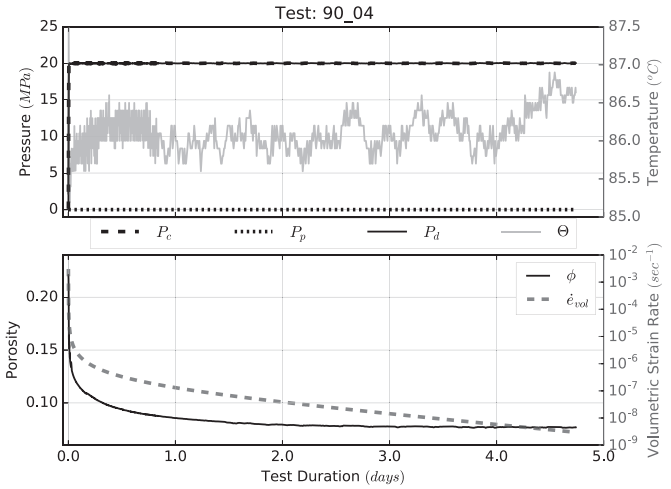

Fig. 2. Measured pressure, temperature, porosity, and volumetric strain rate during experiment 90_04.

pressure, (left) and P_d (center), and the experiments that had both and P_p applied during loading are represented with solid lines (*175_11* and *175_12*). When ϕ is plotted against only (left). Experiments that had nonzero P_p (*175_11* and *175_12*) do not follow the common trend as the experiments with only applied. When these same values of ϕ are plotted against P_d (center), a consistent trend is observed that indicates a yield surface may be defined in terms of the P_d (as shown in the schematic idealization).

During these experiments, only sample *175_13* was subjected to a series of load-unload-reload cycles (Stages 1 through 4), as shown in Fig. 10, and the changes in ϕ during these unload-reload cycles illustrates the inelastic behavior of granular salt. Where, upon unloading during Stages 2 and 4, the change in ϕ was not recovered. Additionally, during Stage 3 (second loading cycle), when was increased from zero to approximately 20 MPa, the reduction in ϕ is negligible and appears to

Table 8
Summary of experiment 175_16.

Stage	Loading	Initial Conditions			Final Conditions			Stage Time	
		P_c (MPa)	P_p (MPa)	P_d (MPa)	P_c (MPa)	P_p (MPa)	P_d (MPa)	Start (day)	Duration (day)
1	Transient	0.0	0.0	0.0	20.0	0.0	20.0	0.000	0.007
2	Creep	20.0	0.0	20.0		———		0.007	5.846
					Total Experiment Time (day):				5.853

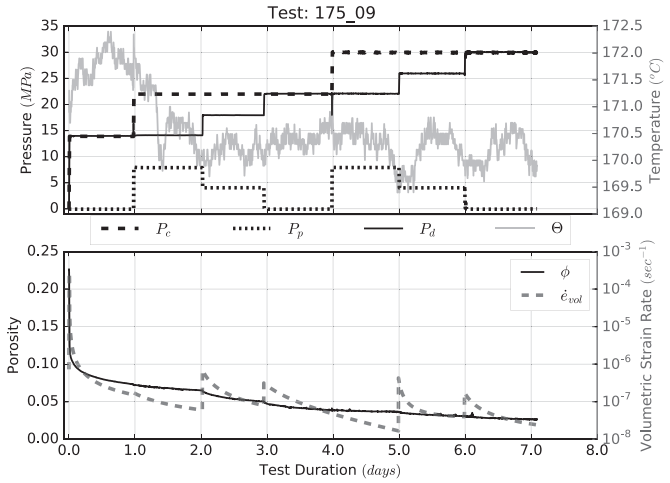

Fig. 3. Measured pressure, temperature, porosity, and volumetric strain rate during experiment 175_09.

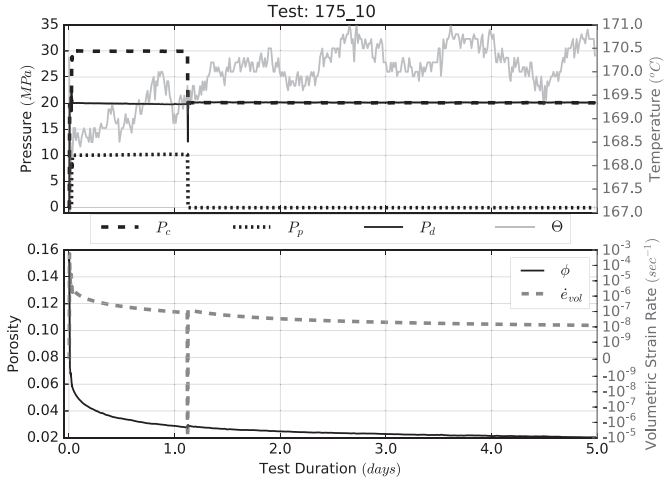

Fig. 4. Measured pressure, temperature, porosity, and volumetric strain rate during experiment 175_10.

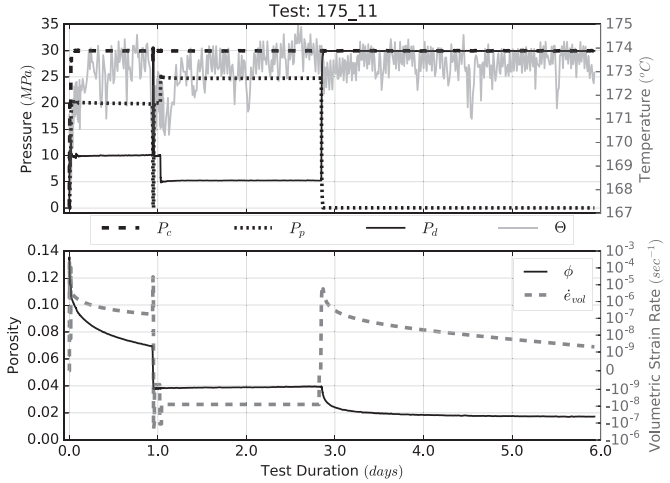

Fig. 5. Measured pressure, temperature, porosity, and volumetric strain rate during experiment 175_11.

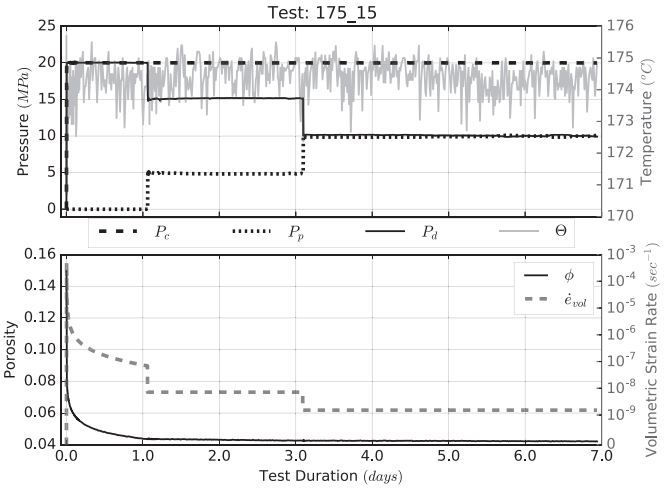

Fig. 6. Measured pressure, temperature, porosity, and volumetric strain rate during experiment 175_15.

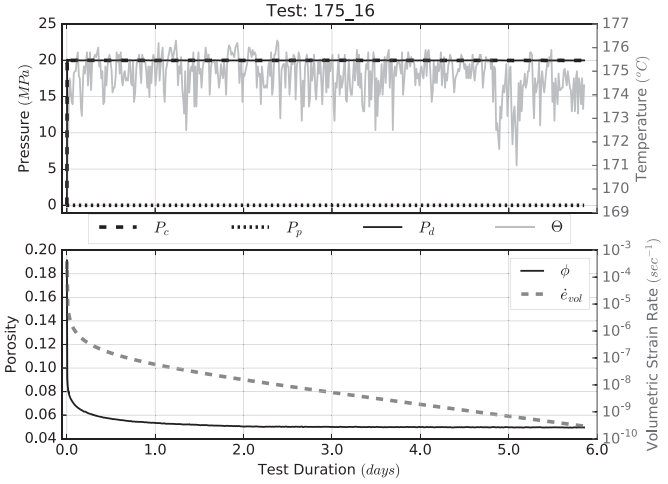

Fig. 7. Measured pressure, temperature, porosity, and volumetric strain rate during experiment 175_16.



Fig. 8. Experimental sample that was cut axially with a diamond saw post test to allow for visual examination of the deformation.

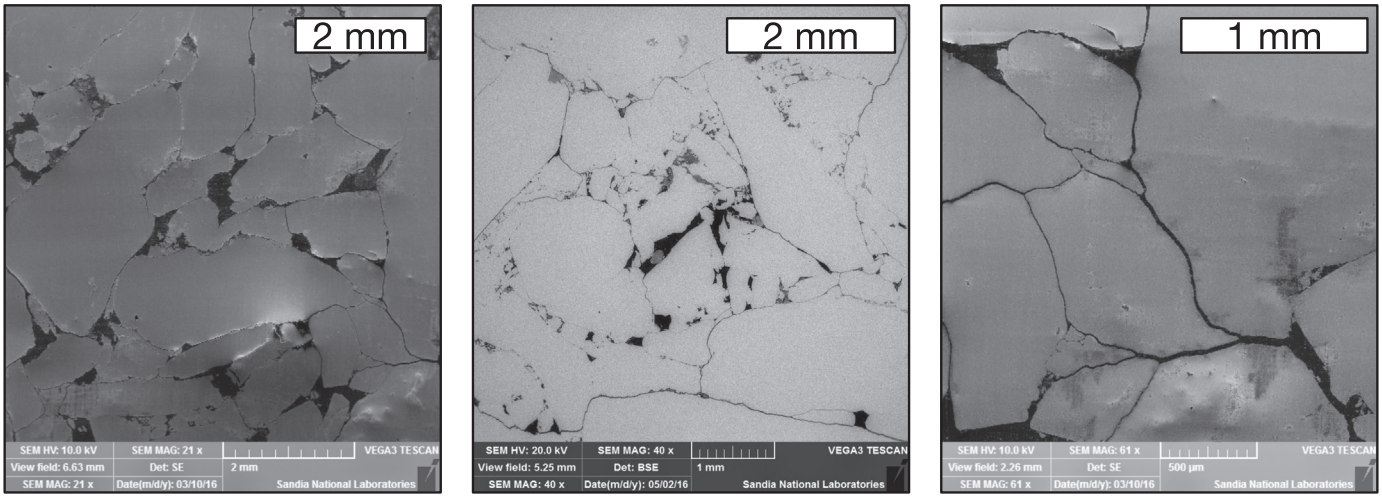

Fig. 9. Series of photomicrographs of granular salt consolidated at 90 °C with $P_c = 20$ MPa and $P_p = 0$ MPa (experiment 90_08); scale bars are located in the upper right corner of each image. Post-test specimen porosity ranged from $\phi = 0.08$ (a and c) to $\phi = 0.03$ (b). Ductile plastic deformation is evident by the suturing of individual salt particles together into a bulk porous material, a process often referred to as *healing* (photomicrographs courtesy of Melissa Mills).

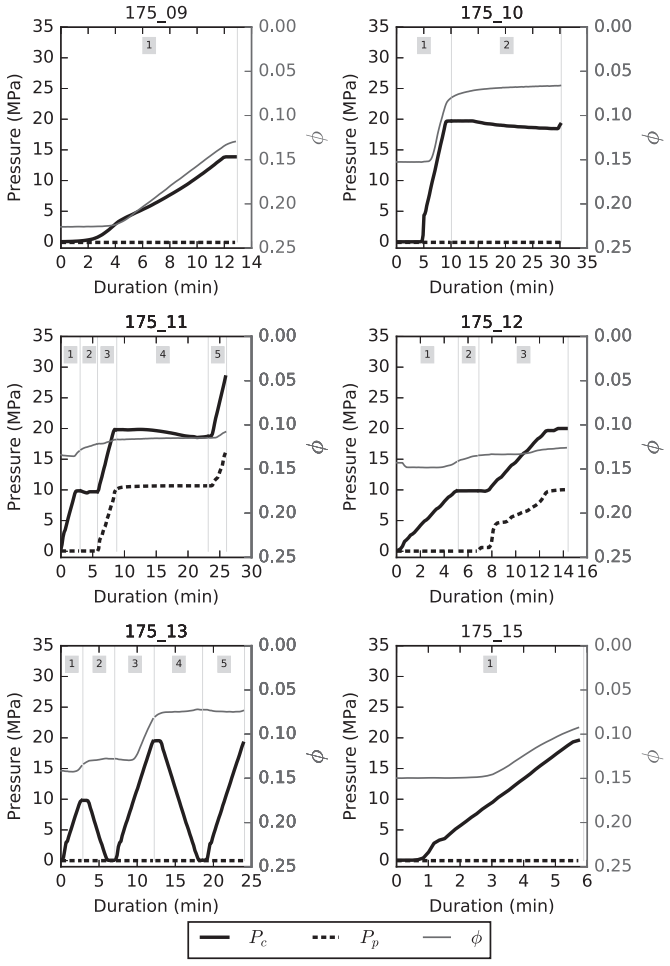

Fig. 10. Experimental results during the initial loading of the *175 series* that illustrate P_c, P_p, and ϕ versus test duration. Numbers along the upper portion of each graph encompassed by a *gray square* identify the test stage.

be elastic until exceeds the previous maximum value that was obtained during Stage 1 ($P_c = 10$ MPa). These results are also illustrated in Fig. 11, where ϕ is plotted against and P_d. Results presented here are consistent with the phenomenon of strain hardening, where the stress level needed to obtain inelastic deformation was increased with inelastic strain.

5.2. Influence of porosity and differential pressure on creep deformation

The field of poromechanics is concerned with studying the deformation of porous materials, such as granular salt, and at the core of poromechanics are the constitutive relations between stress and strain. Biot[13, pg. 156] defined stress within a poroelastic material with the use of a local average over a small but finite area of the porous material that contains both the solid and fluid (pore) phases (i.e., continuum homogenization). The constitutive relations, between stress and strain, proposed by,[13] are absent of a direct reference to the pore volume (e.g., ϕ) within the porous material. However, the experimental results presented here (Section 4) indicated that the stress and strain fields within porous granular salt were directly related to the volume of pore space in the sample (presented in terms of ϕ).

With the experimental results presented here in mind, consider the representation of a porous material in Fig. 12, which illustrates the two discrete phases present in a saturated porous sample along with isostatic loads from the and P_p. The stress field within the fluid phase has only spherical components and can be represented by a scalar value that is equal to P_p; therefore, the fluid phase has no deviatoric components of stress. Alternatively, the solid phase can sustain a general state of stress containing both spherical and deviatoric components. Because an individual particle within a porous material experiences tractions from both the fluid pressure and adjacent particles, the existence of deviatoric stress components within a solid particle is plausible. If two distinct phases exist within a bulk material (fluid and solid), the assumption that a single-isotropic stress field generally exists over the bulk volume is unrealistic.

However, the assumption of a single stress field over a porous material is recognized to be practical when the solid phase is highly resistant to ductile deformation under creep conditions. In such a scenario, a material would undergo either elastic deformation, as Biot[13] assumed, or brittle-plastic deformation. Because salt particles were observed to readily deform in a ductile manner under a constant-isostatic load, assuming the deformations were elastic would not be valid. Recognizing that a fundamental assumption in the theory of poroelasticity did not hold (i.e., reversible deformations), an alternate model was developed to gain insight into the origins that cause ductile

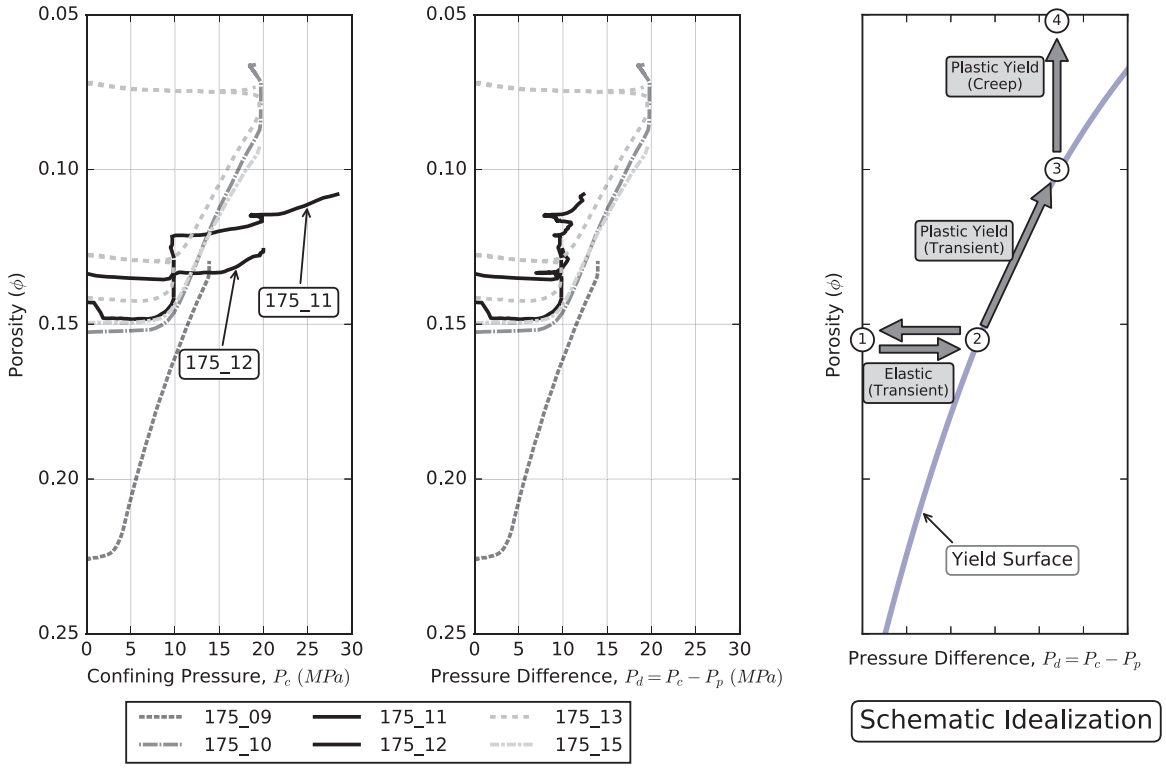

Fig. 11. Experimental results during the initial loading of the *175 series* that illustrate the relationship between ϕ and P_c (left) and ϕ and P_d (center), where experiments that had both P_c and P_p are represented with a solid line. Additionally, a schematic idealization of an apparent hardening curve is illustrated in terms of ϕ and P_d (right).

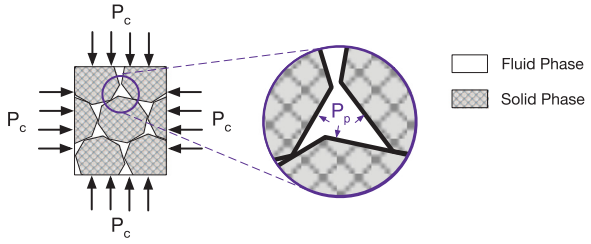

Fig. 12. Graphical representation of a porous material under a P_c and P_p.

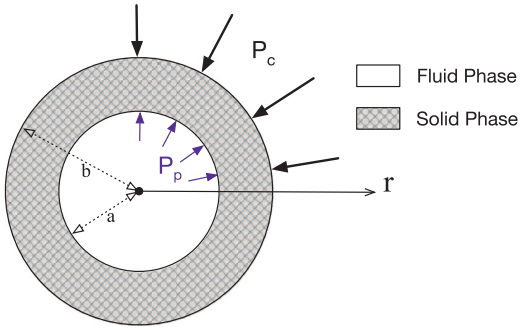

Fig. 13. Chosen RVE for a porous material subjected to P_c and P_p.

deformation of granular salt under isostatic compression.

Consider the smallest volume element of a porous material that exhibits a stress field similar to the bulk specimen, a representative volume element (RVE). Let the geometry of the RVE be that of a thick-walled sphere with an inner radius a and outer radius b, as shown in Fig. 13. Then let the RVE be subjected to and P_p on its outer and inner surfaces, respectively. Under the assumption of isotropic elasticity, the stress distribution over the solid phase is the solution to a classic problem in solid mechanics.[52,53]

The spherical geometry of the chosen RVE allows for the stress-equilibrium solution to be written in terms of the RVE porosity (ϕ_{RVE}), which is conveniently determined from the inner and outer radii as $\phi_{RVE} = (a/b)^3$. The analytical solution to the stress field has two independent components, which are the radial (σ_{rr}) and circumferential ($\sigma_{\theta\theta}$) stress distributions, and these distributions are functions of the macroscopically applied and P_p along with the spherical geometry (in terms of ϕ_{RVE} and a) and the radial coordinate (r), as shown in Eqs. (7) and (8).

$$\sigma_{rr} = \frac{P_c + P_p}{2} + \frac{P_d}{2(1-\phi_{RVE})}\left[1 + \phi_{RVE} - 2\left(\frac{a}{r}\right)^3\right] \tag{7}$$

$$\sigma_{\theta\theta} = \frac{P_c + P_p}{2} + \frac{P_d}{2(1-\phi_{RVE})}\left[1 + \phi_{RVE} + \left(\frac{a}{r}\right)^3\right] \tag{8}$$

Here, σ_{rr} and $\sigma_{\theta\theta}$ represent components of a local stress field over the solid phase that vary with r. The complete stress field is the superposition of the two terms in each of these components, (1) a uniform stress field equal to the average of and P_p, and (2) a spatially variable stress field that results in shear. Notice that the shear stress distribution (i.e., the terms containing r) is dependent upon both ϕ and the P_d, where the uniform (or spherical) stress is independent of ϕ_{RVE}. Therefore, the geometry of the chosen RVE allows for an explicit relationship between the shear stress and ϕ_{RVE} even when the RVE is subjected to macroscopically isotropic stress.

Because the solid phase material of the RVE is assumed to be isotropic, the spherical and deviatoric stress components may be isolated from the total stress tensor for the RVE ($\boldsymbol{\sigma}$). And the spherical part of $\boldsymbol{\sigma}$ may be represented by a scalar measure referred to as the mean stress (σ_m):

$$\sigma_m = \frac{1}{3} tr(\boldsymbol{\sigma}). \tag{9}$$

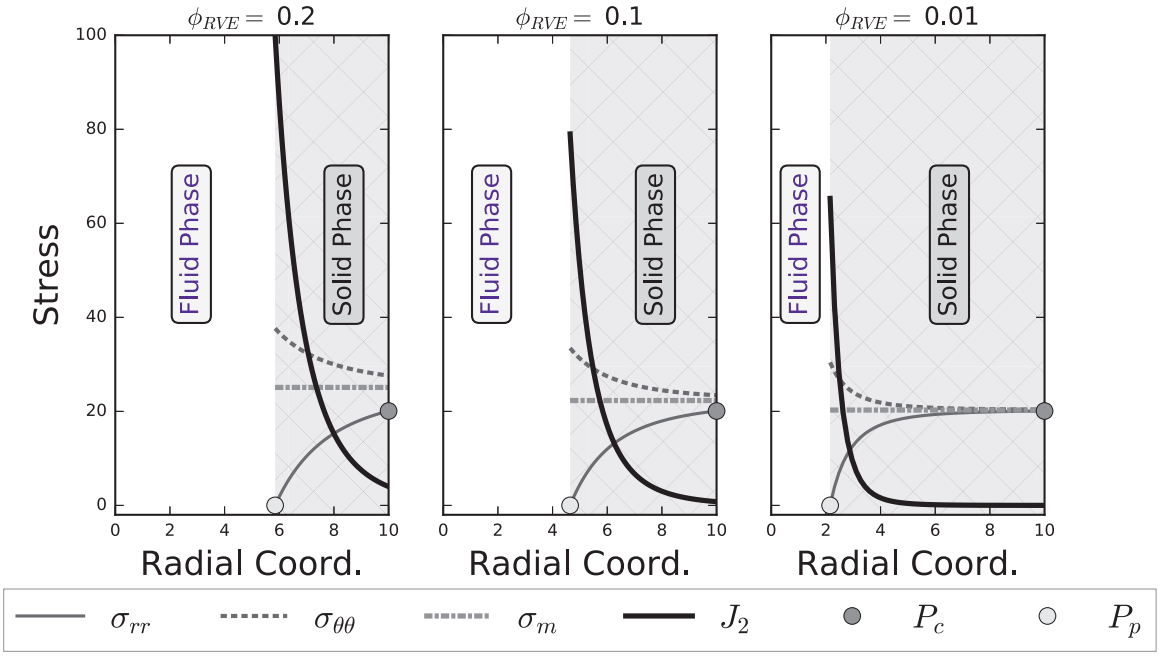

Fig. 14. Normalized stress distribution over the solid phase of the RVE, with constant values of P_c and P_p and variable ϕ, where $\phi = 0.2$ (left), $\phi = 0.1$ (center), and $\phi = 0.01$ (right).

Additionally, the deviatoric stress components of $\boldsymbol{\sigma}$ may be isolated in terms of the stress deviator ($\boldsymbol{\sigma}^{dev}$). The $\boldsymbol{\sigma}^{dev}$, as given in Eq. (10), contains only components that cause shear, and a scalar measure of these shear components is the second invariant of the $\boldsymbol{\sigma}^{dev}$, which is often referred to as the J_2 (Eq. (11)).

$$\boldsymbol{\sigma}^{dev} = \boldsymbol{\sigma} - \frac{1}{3} tr(\boldsymbol{\sigma})\boldsymbol{i} \tag{10}$$

$$J_2 = \frac{1}{2}(\boldsymbol{\sigma}^{dev} \cdot\cdot\, \boldsymbol{\sigma}^{dev}) \tag{11}$$

In Eq. (11), the double dots ($\cdot\,\cdot$) represent the inner product between two second-order tensors. With the use of a spherical RVE, insight into the influence of ϕ on the local shear stress within a porous material may be obtained. Here, the term *local stress* implies the stress field over the solid phase of the RVE (or the experimental specimen it represents), which varies spatially and is not well represented by the macroscopic stresses applied at the boundaries (and P_p). The concept of local stress is depicted in Fig. 14, where the normalized stress distribution, given by Eqs. (7) and (8), versus the normalized radial coordinate is plotted over the solid phase of the spherical RVE. Plotted stresses have been normalized such that the maximum value of J_2 over the solid phase equals 100, and the radial coordinate has been normalized such that the outer radius of the RVE equals 10. Each of the three graphs in Fig. 14 represent an RVE with a unique ϕ_{RVE} that ranges from $\phi_{RVE} = 0.2$ (left) to $\phi_{RVE} = 0.01$ (right), and although each are subjected to the same boundary conditions (and P_p), each has a unique stress distribution.

The practice of assuming an isotropic stress field exists within a porous specimen subjected to isostatic compression is detrimental to understanding the cause of ductile deformation in porous materials; however, recognition of this is not novel. Carroll and Holt[54] performed numerical approximations for the deformation of a thick-walled sphere, and results from these analyses led them to postulate that experimentally observed changes in ϕ were the result of shear stress in the solid phase. Bridgman[55] showed experimentally that ductile deformation of isotropic materials results from a stress field containing shear, and this work confirmed von Mises' theory of Maximum Distortional Energy.[56] Because of these works and many others, the J_2 is often employed in yield criteria to determine the onset of ductile deformation. However, if an isotropic stress field is assumed to exist in a porous material under macroscopically applied isostatic conditions, then the use of J_2 for describing ductile deformation is inhibited. Recognizing the existence of a local stress field, which may deviate from the macroscopically applied fluid pressure, allows for the use of the J_2 under these circumstances. Additionally, an RVE may be adapted to approximate the local stress field and thus provide insight into the fundamental cause of ductile deformation.

Stress distributions presented in Fig. 14 illustrate how the local stresses vary over the domain of the solid phase. The magnitude of J_2 is greatest at the fluid-solid phase interface (pore wall), which indicates that the greatest shear stress will also be at the pore wall along with the greatest amount of shear strain. Although, by definition, shear strain does not cause the volume of the solid phase to alter, it does distort the solid phase. Physical observations presented in Section 4.3 indicated that the bulk sample volume decreased because the pore volume was dramatically reduced, which was the result of the solid particles being distorted and plastically flowing into the pore volume, causing a reduction of ϕ. These observations are consistent with the stress distributions shown in Fig. 14, where shear is concentrated at the pore wall.

The left-most graph in Fig. 14 shows that when the ϕ_{RVE} is sufficiently large, the J_2 is nonzero over the entire solid phase. Whereas the right-most graph in Fig. 14, which depicts results with $\phi_{RVE} = 0.01$, shows that the J_2 rapidly approaches zero as a function of distance from the pore wall. These results illustrate that as ϕ_{RVE} decreases so does the magnitude of the local shear stress in the solid phase. Experimental results presented in Section 4.2 showed the $\dot{e}_{vol}$ decreased as ϕ decreased, and this phenomenon may be explained by recognizing that shear stress within the solid phase of a porous material decreases with ϕ and consequently results in a decreased $\dot{e}_{vol}$. Therefore, the magnitude and variation of local stresses decrease with ϕ, and as ϕ approaches zero the local and macroscopic stress distributions become similar.

Recall the yield surface depicted by the schematic idealization shown on the right in Fig. 11, where the yield surface approached infinite P_d as ϕ approached zero; this too can be explained with the use of the RVE. When $\phi_{RVE} = 0$, the stress distributions given by Eqs. (7) and (8) are equal; therefore, regardless of the magnitude of P_d the $\boldsymbol{\sigma}$ only contains spherical components that produce no shear. Because ductile

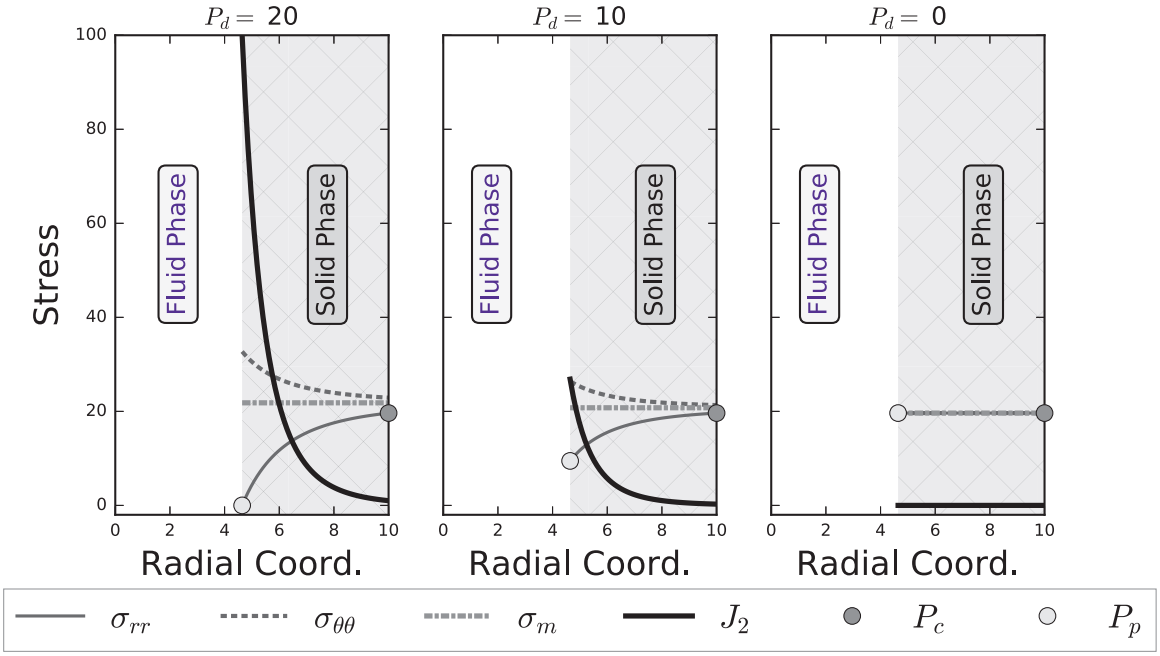

Fig. 15. Normalized stress distribution over the solid phase of the RVE, with constant $\phi_{RVE} = 0.10$ and variable P_d, where $P_d = 20$ (left), $P_d = 10$ (center), and $P_d = 0$ (right).

yielding results from shear, the yield stress can never be obtained under isostatic loading when $\phi_{RVE} = 0$. This line of reasoning is in accordance with the experimental observations.

Consider now the influence of variable P_d only; Fig. 15 illustrates the influence of P_d on the RVE's local stress, where the normalized stress distribution versus the normalized radial coordinate is illustrated for varying levels of P_d. All components of stress have been normalized such that the maximum value of J_2 over the solid phase equals 100, and the radial coordinate has been normalized such that the outer radius of the RVE equals 10. Stress distributions for all three graphs in Fig. 15 were determined with a constant value of $\phi_{RVE} = 0.10$, while the scaled magnitude of P_d ranged from $P_d = 20$ (left), $P_d = 10$ (center) to $P_d = 0$ (right). These three graphs illustrate the direct influence of P_d on the J_2 over the solid phase, where a large P_d results in a greater magnitude of J_2. Experimental results presented in Section 4.2 showed that the $\dot{e}_{vol}$ increased with increasing P_d and decreased with decreasing P_d, and this phenomenon may be understood to occur because the magnitude of shear stress within the solid phase of the bulk granular salt is proportional to the P_d when $\phi_{RVE} \neq 0$. The influence of P_d on the magnitude of shear is highlighted by the right graph of Fig. 15, where the magnitude of $J_2 = 0$ over the entire domain when $P_d = 0$.

The analytical stress distributions considered here also illustrate the influence of ϕ and P_d on σ_m. Fig. 14 shows that σ_m decreases with ϕ_{RVE}, and Fig. 15 illustrates that σ_m decreases with P_d. The influence of ϕ on σ_m was not identified in the experimental work completed here; however, the influence of P_d on the mean stress within the experimental sample was indirectly observed. During multiple experiments (Stage 4 of 175_10; Stages 9, 10 and 11 of 175_11) when the P_d was dropped the sample temporarily exhibited a negative $\dot{e}_{vol}$, which indicates the mean stress on the samples was also reduced. Similar observations have been made during experiments described by Holcomb and Shields[30] and Salzer et al.[9] where the results were interpreted in terms of a Terzaghi type effective stress influence.

The suite of isostatic compression experiments described herein, performed on porous granular salt under isostatic compression, were motivated by a basic understanding that a local stress distribution exists that deviates from the macroscopic stress when $\phi \neq 0$ and $P_p \neq P_c$. A local distribution is typically not considered when evaluating porous geologic materials; however, because salt readily deforms in a ductile manner under very small shear stresses (as described by Berest et al.[57]), the local stress distribution is understood to greatly influence deformation under these circumstances and therefore should be considered. Insight into the fundamental causes of poro-plastic deformation was obtained by considering the analytical solution to the elastic stress-equilibrium problem for a thick-walled sphere. However, considering only the elastic solution to the problem may mask other dominant factors present during inelastic deformation. Therefore, only a high-level insight into the stress distribution is provided here rather than a quantifiable relationship between the macroscopic stress and total deformation. A constitutive model based on a thick-walled spherical RVE would provide quantifiable results that are comparable to the experimentally observed visco-plastic deformation of granular salt under isostatic conditions.

6. Conclusions

A series of isostatic compression experiments were performed to evaluate influence of P_p and ϕ on the ductile deformation of granular salt. These experiments were completed at nominally 90 and 175 °C with independent control of and P_p. Results showed that the $\dot{e}_{vol}$ was influenced by P_p (quantified here in terms of the P_d) and ϕ during both transient and creep loading stages.

During transient loading, plastic yielding was observed to act as function of the P_d and ϕ. Strain hardening was observed to occur as a result of reduced ϕ, and this reduction of ϕ was caused by the ductile flow of the solid particles into the pore space. Deformation during creep loading also depended on both P_d and ϕ. These dependencies were readily observed by changes in the $\dot{e}_{vol}$, where the $\dot{e}_{vol}$ continuously decreased as ϕ decreased. Additionally, by altering the and P_p, the $\dot{e}_{vol}$ was observed as being proportional to the P_d.

The experimentally observed influence of P_d and ϕ on the $\dot{e}_{vol}$ may be understood by incorporating an RVE geometry, and this was done here with a thick-walled spherical RVE. The use of an RVE allowed for a tangible explanation for the development of shear stresses in a porous material under a macroscopically isotropic state of stress. The analytical solution to the stress-equilibrium problem over the RVE was utilized to illustrate the influence of P_d and ϕ on the local stress fields, which may vary from the macroscopically applied and P_p. These results showed

that the J_2 within the solid phase is proportional to P_d, and shear stresses can only exist during isostatic compression when samples have nonzero values of P_d and ϕ.

A major finding of this experimental study was that appreciable shear exists in a porous material under isostatic compression, and the magnitude of shear is influenced by both P_p and ϕ. For modeling purposes, the existence of shear as observed under these circumstances may be captured with the use of a constitutive model that allows for a local stress distribution over an RVE.

Acknowledgments

This material is based upon work supported by the U.S. Department of Energy (DOE) Nuclear Energy University Program (NEUP) Grant Number DE-NE0000733.

Sandia National Laboratories is a multi-mission laboratory managed and operated by National Technology and Engineering Solutions of Sandia, LLC., a wholly owned subsidiary of Honeywell International, Inc., for the U.S. Department of Energy's National Nuclear Security Administration under contract DE-NA0003525.

Appendix A. Supplementary data

Supplementary data associated with this article can be found in the online version at doi:10.1016/j.ijrmms.2018.07.007.

References

1. Hansen FD, Popp T, Wieczorek K, St¨uhrenberg D. *Granular salt summary: Reconsolidation principles and applications. Technical Report SAND2014-1614R, FCRD-UFD-2014-000590Rev. 0*. Albuquerque, NM (United States): Sandia National Laboratories; 2014.
2. Brush L. *Current estimates of gas-production rates, gas-production potentials, and expectedchemical conditions relevant to radionuclide chemistry for the long-term wipp performanceassessment. Sandia Report SAND91-0893/3.* 87185. Albuquerque,New Mexico: Sandia National Laboratories; 1991.
3. Telanderand M, Westerman R. *Hydrogen generation by metal corrosion in simulated wasteisolation pilot plant environments. Sandia Report SAND92-7347*. Albuquerque, New Mexico: Sandia National Laboratories; 1993.
4. Francis A, Gillow J, Giles M. *Microbial gas generation under expected waste isolation pilotplant repository conditions. Sandia Report SAND96-2582*. Albuquerque, New Mexico: Sandia National Laboratories; 1997.
5. Molecke M. Gas generation from transuranic waste degradation. in: Northrup, CJ, editor. Scientific Basis for Nuclear Waste Management. Springer; 1980, p. 569–75. ⟨https://doi.org/10.1007/978-1-4684-3839-0⟩.
6. Spiers C, Brzesowsky R. Densification behaviour of wet granular salt: Theory versus experiment. In: Proceedings of the Seventh Symposium on Salt, vol. 1. Elsevier Amsterdam; 1993:83–92.
7. Callahan GD, Mellegard KD, Hansen FD. Constitutive behavior of reconsolidating crushed salt. *Int J Rock Mech Min Sci.* 1998;35:422–423.
8. Olivella S, Gens A. A constitutive model for crushed salt. *Int J Numer Anal Methods Geomech.* 2002;26:719–746.
9. Salzer K, Popp T, Böhnel H. Mechanical and permeability properties of highly precompacted granular salt bricks. In: Proceedings of the 6th Conference on the Mechanical Behavior of Salt, Hannover, Germany; 2007:239–48.
10. Czaikowski O, Wieczorek K, Kröhn K. Compaction of salt backfill-new experiments and numerical modelling. In: Bérest, P, Ghoreychi, M, Hadj-Hassen, F, Tijani, M, editors. Proceedings of the 7th Conference on the Mechanical Behaviour of Salt, vol. 7 of Mechanical Behaviour of Salt; 2012:155–60.
11. Terzaghi K. The shearing resistance of saturated soils and the angle between the planes of shear. In: Proceedings of the 1st International Conference on Soil Mechanics and Foundation Engineering, vol. 1. Cambridge, MA: Harvard University Press; 1936:54–6.
12. Fillunger P. Versuche über die Zugfestigkeit bei allseitigem Wasserdruck. *Osterr Wochenschr Offentl Baudienst.* 1915;29:443–448.
13. Biot MA. General theory of three-dimensional consolidation. *J Appl Phys.* 1941;12:155–164. https://doi.org/10.1063/1.1712886.
14. Nur A, Byerlee J. An exact effective stress law for elastic deformation of rock with fluids. *J Geophys Res.* 1971;76(26):6414–6419.
15. Murphy G. *Advanced Mechanics of Materials.* McGraw-Hill Book Company, inc.; 1946.
16. Stormont J. Gas permeability changes in rock salt during deformation. Ph.D. Thesis; University of Arizona; Tuscon, AZ; 1990.
17. Fokker P, Kenter C, Rogaar H. The effect of fluid pressures on the mechanical stability of (rock) salt. In: Proceedings 7th Symposium on Salt, Elsevier Science Publication; 1993.
18. Pfeifle T, Hurtado L. Effect of pore pressure on damage accumulation in salt. in: Geertman, RM, editor. Eigth Salt Symposium vol. 8. Elsevier; 2000:307–12.
19. Biot M, Willis D. The elastic coefficients of the theory of consolidation. *J Appl Mech.* 1957;24:594–601.
20. Skempton A. Effective stress in soils, concrete and rocks. In: Proceedings of Conference on Pore Pressure and Suction in Soils. Selected papers on soil mechanics; International Society of Soil Mechanics and Foundation Engineering; London, Butterworths; 1960:4–16.
21. Wang H. *Theory of Linear Poroelasticity with Applications to Geomechanics and Hydrogeology.* Princeton University Press; 2000.
22. Terzaghi K. Theoretical soil mechanics; vol. 18. Wiley Online Library; 1943.
23. McTigue D. Thermoelastic response of fluid-saturated porous rock. *J Geophys Res: Solid Earth.* 1986;91(B9):9533–9542.
24. Skempton A. The Pore-pressure Coefficients a and b. *Selected Papers on Solid Mechanics.* Thomas Telford Publishing; 1984:65–69.
25. Wang H. Experimental error for permeability and specific storage from pulse deca measurements. *Int J Rock Mech Min Sci Geomech Abstr.* 1993;30(7):1173–1176.
26. Alkan H, Cinar Y, Pusch G. Rock salt dilatancy boundary from combined acoustic emission and triaxial compression tests. *Int J Rock Mech Min Sci.* 2007;44(1):108–119.
27. Kansy A. Influence of biot parameter on the hydraulic behvior of rock salt taking into acount the pore pressure (translated from german). Ph.D. Thesis; Original title: Einfluss des Biot-Parameters auf das hydraulische Verhalten von Steinsalz unter der Berücksichtigung des Porendruckes, Institute of Petroleum Engineering TU Clausthal; 2007. URL ⟨https://books.google.com/books?Id=dbcUjwEACAAJ⟩.
28. Shor A, Baes CJ, Canonico C. Consolidation and permeability of salt in brine. Tech. Rep. ONRL-5774; Oak Ridge National Laboratory; Oak Ridge, Tennessee; 1981.
29. Holcomb D, Hannum D. *Consolidation of crushed-salt backfill under conditions appropriateto the WIPP facility. Sandia Report SAND82-0630.* Albuquerque, New Mexico: Sandia National Laboratories; 1982.
30. Holcomb D, Shields M. *Hydrostatic creep consolidation of crushed salt with added water. Sandia Report SAND87-1990.* Albuquerque, New Mexico 87185: Sandia National Laboratories; 1987.
31. Spiers CJ, Peach CJ, Brzesowsky RH, Schutjens P, Liezenberg J, Zwart H. Long-term rheological and transport properties of dry and wet salt rocks. Commission on the European Communities: Nuclear Science and Technology EUR 11848; Department of Geology, University of Ultrecht; PO Box 80.021, Ultrecht, The Netherlands; 1988.
32. Zeuch D, Zimmerer D, Shields M. *Interim report on the effects of brine-saturation and shear stress on consolidation of crushed, natural rock salt from the waste isolation pilot plant (WIPP). Sandia Report SAND91-0105.* Albuquerque, New Mexico 87185: Sandia National Laboratories; 1991.
33. Zeuch D, Holcomb D. *Experimental and modeling results for reconsolidation of crushed natural rock salt under varying physical conditions. Sandia Report SAND90-2509.* Albuquerque, New Mexico 87185: Sandia National Laboratories; 1991.
34. Brodsky, NS. Hydrostatic and shear consolidation tests with permeability measurements onwaste isolation pilot plant crushed salt. Contractor Report by RE/SPEC inc. SAND 93-7058;1994.
35. Bechthold W, Rothfuchs T, Poley A, Ghoreychi M, Heusermann S, Gens A, et al. *Backfilling and sealing of underground repositories for radioactive waste in salt. BAMBUS Project EUR 19124 EN*. European Commission – Nuclear Science and Technology; 1999.
36. Bechthold W, Smailos E, Heusermann S, Bollingerfehr W, Bazargan Sabet B, Rothfuchs T, et al. Backfilling and sealing of underground repositories for radioactive waste in salt. BAMBUS-II Project 20621; Commission of the European Communities, EUR; 2004.
37. Kröhn K, Zhang C, Wolf J, et al. The compaction behaviour of salt backfill at low porosities. *Mech Behav Salt VII.* 2012:161.
38. Kröhn K, Zhang C, Czaikowski O, Stührenberg D, Heeman U. The compaction behaviour of salt backfill as a thm-process. In: Roberts, L, Mellegard, K, Hansen, F, editors. The Mechanical Behavior of Salt VIII; vol. 8. CRC press; 2015, p. 49–59.
39. Callahan GD. Crushed salt constitutive model. Contractor Report by RE/SPEC inc. SAND 98-2680; Sandia National Laboratories; 1999.
40. Broome S, Bauer S, Hansen F, Mills M. Mechanical response and microprocesses of reconsolidating crushed salt at elevated temperature. *Rock Mech Rock Eng.* 2015;48(6):2615–2629.
41. Holcomb DJ, Zeuch DH. Modeling the consolidation of a porous aggregate of dry salt as isostatic hot pressing. *J Geophys Res: Solid Earth.* 1990;95(B10):15611–15622.
42. Ashby M, Frost H. *Deformation-Mechanism Maps.* Oxford: Pergamon Press; 1982.
43. Robertson E, Robie R, Books K. Physical properties of salt, anhydrite, and gypsum. Trace Elements Memorandum Report 1048; US Department of the Interior, Geological Survey; 1958.
44. Schuler KW. Lateral-deformation gage for rock-mechanics testing. *Exp Mech.* 1978;18(12):477–480.
45. Brodsky N, Hansen F, Pfeifle T. Properties of dynamically compacted waste isolation pilot plant salt. In: Michel Aubertin, HRH, editor. In: Proceedings of the 4th Conference on Mechanical Behaviour of Salt SAND96–0838C; Trans Tech; 1996.
46. Paneru L. Measurement of thermal properties and porosity of consolidated salt. Master's thesis; University of New Mexico; 2016. URL ⟨http://digitalrepository.unm.edu/ce_etds/127⟩.
47. Pennock G, Zhang X, Peach CJ, Spiers CJ. Microstructural study of reconsolidated salt. In: Wallner, M, Lux, KH, Minkley, W, Hardy Jr, H, editors. The Mechanical Behavior of Salt - Understanding the THMC Processes in Salt; vol. SaltMech6. Hannover, Germany: Taylor and Francis; 2007, p. 231–7.
48. Mowar S, Zaman M, Stearns D, Roegiers JC. Micro-mechanisms of pore collapse in limestone. *J Pet Sci Eng.* 1996;15(2–4):221–235.
49. Munson D, Dawson P. *Constitutive model for the low temperature creep of salt (with applicationto WIPP). Sandia Report SAND79-1853*. Albuquerque, New Mexico: Sandia National Laboratories; 1979.
50. Munson D, Fossum A, Senseny P. Advances in resolution of discrepancies between predicted and measured in situ WIPP room closures. Sandia Report SAND88-2948; Sandia National Laboratories and Southwest Research Institute and RE/SPEC inc.; 1989.
51. Troyer KL, Estep DJ, Puttlitz CM. Viscoelastic effects during loading play an integral role in soft tissue mechanics. *Acta Biomater.* 2012;8(1):234–243.
52. Love A. A treatise on the mathematical theory of elasticity. 1944.

53. Timoshenko S, Goodier J. Theory of elasticity; 1951.
54. Carroll M, Holt A. Static and dynamic pore-collapse relations for ductile porous materials. *J Appl Phys.* 1972;43(4):1626–1636.
55. Bridgman PW. *Studies in large plastic flow and fracture.* New York: McGraw-Hill; 1952.
56. Bohannan P. Selected papers of richard von mises; 1965.
57. Berest P, Béraud JF, Bourcier M, Dimanov A, Gharbi H, Brouard B, et al. Very slow creep tests on rock samples. In: Proceedings of the Mechanical Behavior of Salt, VII, 2012:81–8.